

Coherently manipulating triplet-exciton qubit by circularly polarized laser

Longlong Zhang(张龙龙), Hongwei Li(李宏伟), Zhenyu Xu(徐振宇), Mengze Tao(陶孟泽), Rui Chen(陈睿), and Yingqi Ma(马英起)

Citation: Chin. Phys. B, 2026, 35 (**7**): 070303. DOI: 10.1088/1674-1056/ae1450
http://cpb.iphy.ac.cn; http://iopscience.iop.org/cpb

What follows is a list of articles you may be interested in

Quantum toric code decoding method based on syndrome-preliminary error fusion module and ResNet architecture

Nai-Hua Ji(纪乃华), Ping-Li Song(宋平俐), Wei Wang(王伟), Hui-Qian Sun(孙汇倩), and Hong-Yang Ma(马鸿洋)
Chin. Phys. B, 2026, 35 (**6**): 060303. DOI: 10.1088/1674-1056/ae1818

Experimental demonstration of quantum optimal control via the alternating control-evolution protocol

Ruiqi Tang(汤睿琪), Yanjun Hou(侯彦君), Zhenyue Du(杜臻越), Zhuoyue Xu(徐卓越), Yuquan Chen(陈昱全), Zhaokai Li(李兆凯), and Xinhua Peng(彭新华)
Chin. Phys. B, 2026, 35 (**6**): 060302. DOI: 10.1088/1674-1056/ae56e0

Distributed quantum circuit partitioning and teleportation optimization based on a multi-dimensional evaluation strategy

Le Zhang(张乐), Zhijin Guan(管致锦), Shuo Qin(秦硕), Zheng Luo(罗政), Fei Ding(丁飞), and Xueyun Cheng(程学云)
Chin. Phys. B, 2026, 35 (**5**): 050305. DOI: 10.1088/1674-1056/ae1c30

Auxiliary-qubit-free quantum approximate optimization algorithm for the minimum dominating set problem

Guanghui Li(李广辉), Xiaohui Ni(倪晓慧), Junjian Su(苏俊健), Sujuan Qin(秦素娟), Fenzhuo Guo(郭奋卓), Bingjie Xu(徐兵杰), Wei Huang(黄伟), and Fei Gao(高飞)
Chin. Phys. B, 2026, 35 (**5**): 050304. DOI: 10.1088/1674-1056/ae5052

Quantum computation and simulation with vibrational modes of trapped ions

Wentao Chen(陈文涛), Jaren Gan, Jing-Ning Zhang(张静宁), Dzmitry Matuskevich, and Kihwan Kim(金奇奂)
Chin. Phys. B, 2021, 30 (**6**): 060311. DOI: 10.1088/1674-1056/ac01e3

Coherently manipulating triplet-exciton qubit by circularly polarized laser

Longlong Zhang(张龙龙), Hongwei Li(李宏伟), Zhenyu Xu(徐振宇),
Mengze Tao(陶孟泽), Rui Chen(陈睿), and Yingqi Ma(马英起)†

State Key Laboratory of Space Weather, National Space Science Center, Chinese Academy of Sciences, Beijing 100190, *China*

(Received 26 June 2025; revised manuscript received 1 October 2025; accepted manuscript online 17 October 2026)

We theoretically propose a scheme for the coherent manipulation of a single qubit, which is constructed using the self-trapped triplet exciton (STTE) in FM/polymer/FM sandwich. The STTE serves as a quantum dot, comprising two degenerate triplet states with opposite magnetizations, thereby forming the qubit's subspace. We demonstrate that the spin state of this qubit can be coherently manipulated by applying an external circularly polarized laser (CPL) to form the Floquet state. The manipulation exhibits significant helicity dependence: when the CPL's angular momentum is antiparallel to the STTE's spin orientation, the STTE undergoes Rabi oscillations between the $|\uparrow\uparrow\rangle$ and $|\downarrow\downarrow\rangle$ state, corresponding to a π-rotation around the x-axis on the Bloch sphere. Conversely, when the CPL's angular momentum is parallel to the STTE's spin orientation, the STTE remains unresponsive to the CPL. Two-axis coherent control of the STTE qubit can be potentially realized by additionally applying a static magnetic field B_z. Our work provides a theoretical perspective for realizing the coherent manipulation of a qubit in organic devices.

Keywords: triplet exciton, coherent manipulation, qubit, circularly polarized laser

PACS: 03.67.Lx, 85.75.–d, 71.35.Lk

DOI: 10.1088/1674-1056/ae1450 **CSTR:** 32038.14.CPB.ae1450

1. Introduction

The fundamental building block of quantum information processing is the quantum bit, *i.e.*, qubit.[1] Unlike the classical bit, which exists in a binary state (0 or 1), a qubit can exist in a superposition of two quantum states. Over the years, various types of qubits have been developed in semiconductor devices, many of which are based on spin states.[2–8] However, one common challenge for spin-based qubits is their susceptibility to decoherence due to spin–orbit coupling.[9,10] To address this issue, organic semiconductors offer a promising solution. Organic materials exhibit weak spin–orbit coupling, leading to longer spin coherence lifetime, potentially reaching microsecond scales.[11] A recent study has proved that the oriented triplet excitons in molecular donor–acceptor single cocrystal can function as long-lived spin qutrits.[12]

In organic semiconductors, the spin states of an exciton include one singlet S $\left[\left(1/\sqrt{2}\right)\left(|\uparrow\downarrow\rangle - |\downarrow\uparrow\rangle\right)\right]$ and three degenerate triplet states $|T_+\rangle$ ($|\uparrow\uparrow\rangle$), $|T_-\rangle$ ($|\downarrow\downarrow\rangle$), and $|T_0\rangle$ $\left[\left(1/\sqrt{2}\right)\left(|\uparrow\downarrow\rangle + |\downarrow\uparrow\rangle\right)\right]$. The energy difference between the singlet and triplet states can be as large as 0.7 eV,[13] making it challenging to drive coherent rotations between these states. To overcome this challenge, we propose a strategy to construct a qubit subspace using the degenerate T_+ and T_- states, enabling coherent manipulation of the spin states. Figure 1 illustrates a prototype initializing a $|T_+\rangle$–$|T_-\rangle$ qubit in a polymer sandwiched between two ferromagnetic (FM) electrodes. The magnetism of the two FM electrodes is aligned parallel by an external magnetic field. By tuning the chemical potential of the FM electrodes, spin-polarized electrons and holes are injected into the polymer layer, maintaining their initial polarization during transport.[11] Upon encountering each other, the electron and hole form a triplet exciton, which can become self-trapped due to the confinement from the Coulomb interactions and the electron–lattice coupling. This self-trapped triplet exciton (STTE) qubit is non-radiative and resistant to dissociation into free charges, allowing the initial state to be maintained for extended periods.

The question then arises: how can we coherently control this STTE qubit? Given that all-optical coherent control of excitonic qubits has been successfully demonstrated in previous studies,[14–16] we propose using a circularly polarized laser (CPL) to achieve coherent manipulation of the STTE qubit. The $|T+\rangle$ and $|T_-\rangle$ states have net S_z and form a two-level system. They are sensitive to the magnetic field as well as the effective magnetic field generated by CPL via the inverse Faraday effect. The CPL's angular momentum could interact with the net spin, and thus, coherent control is realizable. In Fig. , we demonstrate two distinct configurations for applying the CPL: one is that the angular momentum of CPL is antiparallel to the spin orientation of STTE [Fig. 1(a)], and the other is that the angular momentum of CPL is parallel to the spin orientation of STTE [Fig. 1(b)]. We will theoretically show that the responses of the STTE qubit's states are markedly different in

†Corresponding author. E-mail: myq@nssc.ac.cn

© 2026 Chinese Physical Society and IOP Publishing Ltd. All rights, including for text and data mining, AI training, and similar technologies, are reserved.

these two scenarios.

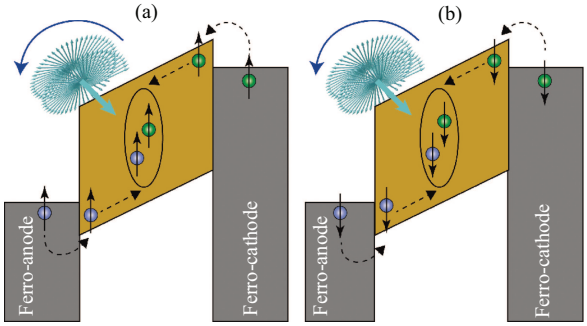


Fig. 1. Schematic illustration of the prototype of the FM/polymer/FM sandwitch used to initialize the STTE qubit. An external CPL is applied to coherently manipulate the spin state of STTE in two configurations: (a) the angular momentum of CPL is antiparallel to the spin orientation, (b) the angular momentum of CPL is parallel to the spin orientation.

2. Theoretical model

To model this behavior, we use the parameters of poly-paraphenylenevinylene (PPV) as a representative organic semiconductor. The Hamiltonian of PPV's electronic system under the CPL irradiation is given by[17]

$$\mathcal{H}(t) = \mathcal{H}_0(t) + \mathcal{H}_{\rm cp}(t), \tag{1}$$

$$\begin{aligned}\mathcal{H}_0(t) = &-\sum_i t_i \left(c_i^\dagger c_{i+1} + \text{h.c.}\right) + \frac{K}{2}\left(u_{i+1}^2 - u_i^2\right) \\ &+ \frac{M}{2}u_i^2 + U\sum_i \left(n_{i,\uparrow} - \frac{1}{2}\right)\left(n_{i,\downarrow} - \frac{1}{2}\right) \\ &+ V\sum_i\sum_{s,s'}(n_{i,s} - 1)(n_{i+1,s'} - 1),\end{aligned} \tag{2}$$

$$\mathcal{H}_{\rm cp}(t) = \sum_i B\left(\mathrm{e}^{-\mathrm{i}\omega t}c_{i\uparrow}^\dagger c_{i\downarrow} + \mathrm{e}^{\mathrm{i}\omega t}c_{i\downarrow}^\dagger c_{i\uparrow}\right), \tag{3}$$

where $\mathcal{H}_0(t)$ is the Su–Schriffer–Heeger (SSH) Hamiltonian[18,19] including the Coulomb interactions. The quantity t_i is given by $t_i = \{t_0 + (-1)^i t_1 + \alpha[u_{i+1}(t) - u_i(t)]\}$ with t_0 the π-electronic hopping integrals in a regular lattice, α the electron–lattice (EL) coupling constant, and u_i the lattice displacement of the atom at i-th site from its equidistance positions. The quantity t_1 is to lift the ground-state degeneracy for nondegenerate polymers. Operators $c_{i,s}^\dagger$ ($c_{i,s}$) creates (annihilates) a π electron with spin s at site i; K denotes the spring constant of the σ bond and M is the mass of a CH group. U gives the strength of the on-site Coulomb interactions while inter-site ones are modeled in $V_{i,i+1} = U/\kappa\sqrt{1 + 0.6117a_0^2}$; $\kappa = 1$ reads as a dielectric parameter and a reads as the distance constance. Defining the bond-length change $y_i = u_{i+1} - u_i$ (u_i is the replace of the i-th atom), the ground state turns out the dimerized bond orders, which is obtained by self consistently solving Eq. (2) and the Hellman–Feyman equation $y_i = (-2\alpha/K)\left[\sum_s \langle c_{i,s}^\dagger c_{i,s}\rangle - (1/N)\sum_{i,s}\langle c_{i,s}^\dagger c_{i,s}\rangle\right]$. We define the alternative component of bond orders $\tilde{y}_i = (-1)^i(2y_i - y_{i-1} - y_{i+1})$ for easy observation. The bound exciton is simulated by setting electron–hole pairs to occupy the spin-associate the highest occupied molecular orbital (HOMO) and the lowest unoccupied molecular orbital (LUMO) levels. Setting the parameters as $t_0 = 2.5$ meV, $t_1 = 0.2t_0$, $U = 1.0t_0$, $a_0 = 1.0$, $K = 1.0$, $\alpha = 0.7t_0$,[19,20] the STTE is stabilized with the binding energy estimated as $E_{\rm binding} = 0.52t_0$.

Equation (3) describes the interactions between CPL and the spins of π electrons. Spins undergo flipping while absorbing circularized photons. The variable ω denotes the frequency of the CPL while B is the strength of the CPL-induced effective magnetic field. Note that when the CPL is applied, Eq. (1) satisfies $\mathcal{H}(t) = \mathcal{H}(t + T)$, where $T = 2\pi/\omega$. This indicates that the exciton state governed by Eq. (1) becomes the Floquet state. Furthermore, given that the wavelength of CPL is longer than the chain length, the effect of CPL is uniformly applied to every site. Equation (3) can be expressed as $\mathcal{H}_{\rm cp}(t) = \sum_i B(\cos\omega t s_{i,x} + \sin\omega t s_{i,y})$, indicating a left-handed helical polarization.[20] The evolution of the electronic system is obtained by integrating the following Schrödinger equation:

$$\mathrm{i}\hbar\dot{\Psi}(t) = \mathcal{H}^{\rm HF}(t)\Psi(t), \tag{4}$$

where $\mathcal{H}^{\rm HF}(t)$ represents the Hartree–Fock (HF) approximation of Eq. (1) and $\Psi(t)$ denotes the many-body wave function constructed from the one-particle HF orbitals. Discretizing the time variables as $t_j = j\Delta t$, we directly integrate Eq. (4) stepwise[21,22]

$$\Psi_\mu(t_{j+1}) = \mathcal{T}\exp\left[-\frac{1}{\hbar}\int_{t_j}^{t_j+\Delta t}\mathcal{H}^{\rm HF}\mathrm{d}t\right]\Psi_\mu(t_j), \tag{5}$$

where $\mathcal{T}$ denotes the time-ordering operator.

The STTE-associated HF orbitals are separated from the continuous bands and they can be treated as a two-level quantum dot system. For two electrons (labeled as 1 and 2) occupying the two HF orbitals (labeled as a and b), the exciton state can be expressed as[23]

$$\begin{aligned}|\Phi_{\rm EX}(t)\rangle = &\frac{1}{\sqrt{2}}\{[\phi_{1,a\uparrow}(t)\alpha_1 + \phi_{1,a\downarrow}(t)\beta_1][\phi_{2,b\uparrow}(t)\alpha_2 \\ &+ \phi_{2,b\downarrow}(t)\beta_2] - [\phi_{2,a\uparrow}(t)\alpha_2 + \phi_{2,a\downarrow}(t)\beta_2][\phi_{1,b\uparrow}(t)\alpha_1 \\ &+ \phi_{1,b\downarrow}(t)\beta_1]\}.\end{aligned} \tag{6}$$

The time-dependent fractions of the $|T_+\rangle$ and $|T_-\rangle$ components are $f_X(t) = \langle X|\Phi_{\rm EX}(t)\rangle$ ($X = |T_+\rangle, |T_-\rangle$).

3. Results and discussion

Figure 2 illustrates the time evolution of $f_X(t)$ for $X = |T_+\rangle, |T_-\rangle$ when the STTE is irradiated by a CPL. The CPL's angular momentum is either (a) antiparallel or (b) parallel to the STTE spin orientation. The CPL is introduced at 0.05 ns, and unless otherwise noted, the CPL parameters are set to $\omega = 0.1t_0$ and $B = 0.06t_0$. In Fig. 2(a), we observe that the CPL drives Rabi oscillation between the $|T_+\rangle$ and $|T_-\rangle$ components of the STTE spin state. The Rabi oscillation frequency is estimated to be approximately 30 GHz and maintained for

about 0.45 ns. Tuning ω can significantly affect the Rabi oscillation characteristics. Decreasing ω reduces the Rabi oscillation frequency and shortens the coherence time. For example, at $\omega = 0.01t_0$, the Rabi oscillation frequency drops to approximately 10 GHz, and the coherence between $|T_+\rangle$ and $|T_-\rangle$ decays rapidly. In contrast, increasing ω nonlinearly increases the Rabi oscillation frequency and extends the coherence time. For instance, at $\omega = 0.2t_0$, the Rabi oscillation frequency rises to about 50 GHz, and the coherence between $|T_+\rangle$ and $|T_-\rangle$ is correspondingly preserved for a longer time.

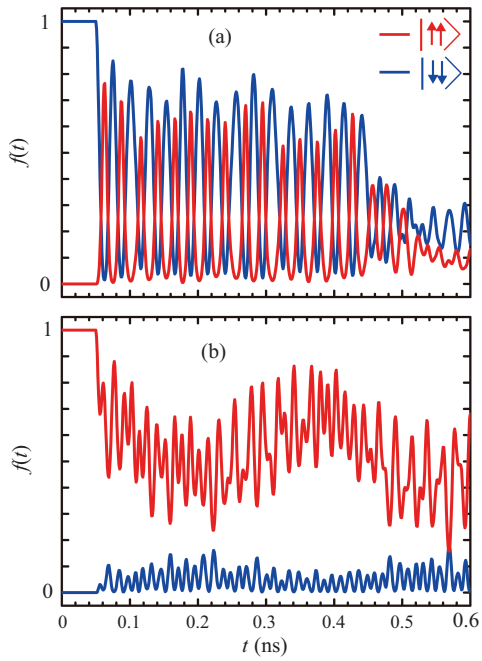


Fig. 2. (a) Rabi oscillation between $|T_+\rangle$ and $|T_-\rangle$ states while setting the angular momentum of CPL antiparallel to initial spin state of STTE, (b) STTE weakly response to the CPL while their angular momentum are parallel to each other, for $\omega = 0.1$, $B = 0.06$, unless otherwise noted.

On the other hand, the field amplitude B also significantly influences the manipulation features of the STTE qubit. When B is small ($B \ll 0.01t_0$), the initial state T_+ is conserved with no observable spin switching. While B reaches a threshold about $B \approx 0.01t_0$, the Rabi oscillations are triggered, making the onset of coherent manipulation. The threshold could be related to the type of polymer material due to various Coulomb and EL interaction strengths. The stronger interaction leads to higher localization of the qubit and stronger spin coherence. When the interactions are too weak, the trapping structure is destroyed and the spins become almost insensitive to the CPL. Beyond the threshold, increasing B will nonlinearly increase the Rabi oscillation frequency. However, since $H_{\rm cp}(t)$ acts as the oscillating magnetic field in the x–y plane, it provides spin-mixing and opens the avenue for the triplet-singlet conversion. Further increasing B enhances the spin mixing effect, and eventually causes the triplet-singlet conversion ratio to become larger, which leads to the reduction of the Rabi oscillation amplitude. The observed behavior indicates that the Rabi oscillations are a coherent phenomenon resulting from the interaction between the quantum dot (QD) system and the oscillating electromagnetic field of the CPL. Consequently, this allows for efficient storage of the information carried by the CPL within the quantum system.

Figure 2(b) demonstrates that when the angular momentum of CPL is parallel to the STTE spin orientation, the initial spin state cannot be switched to its opposite. This highlights the significant helicity-dependence of STTE manipulation by CPL, and introduces the controllable parameter for manipulating and detecting the STTE qubit: (i) In an assumed STTE qubit array, one can precisely determine which qubits can be manipulated by setting their initial spin orientations. This allows for selective control over specific qubits within the array. (ii) For a state-unknown STTE qubit, a circularly polarized probe pulse can be applied to infer the spin state by analyzing the photoresponse dynamics. It is worth noting that helicity-dependent manipulation is a unique characteristic of using CPL to control the STTE qubits. Assuming $\omega = 0$, the Hamiltonian of $\mathcal{H}_{\rm cp}$ reduces to interactions between spins of π-electrons and the static magnetic field along the x-axis. Under such circumstances, regardless of the initial spin orientation, the evolutions of $f_X(t)$ exhibit identical oscillation features for either $|T_+\rangle$ or $|T_-\rangle$ initial state, and the helicity-dependent behaviour disappears.

Figure 3(a) displays the Bloch sphere constructed using the $|T_+\rangle$ and $|T_-\rangle$ states. The pure state on the surface of the Bloch sphere is expressed as $|\psi\rangle = \cos(\theta/2)|T_+\rangle + e^{i\phi}\sin(\theta/2)|T_-\rangle$, where θ (ϕ) denotes the angle between $|\psi\rangle$ and z (x) axis. The north and south poles correspond to the $|T_+\rangle$ and $|T_-\rangle$ states, respectively, while the A and B points on the equator represent the superposition states: $(1/\sqrt{2})(|T_+\rangle - |T_-\rangle)$ and $(1/\sqrt{2})(|T_+\rangle + |T_-\rangle)$. Using the setup illustrated in Fig. 1, the initial state of the STTE qubit can be set to either T_+ or T_-. When excited by a CPL, the initial state's behavior depends on the CPL's angular momentum. The Rabi oscillation revealed in Fig. 2(a) corresponds to the rotation around x-axis, which is shown in Fig. 3(b). Its instantaneous spin state during the rotation is further demonstrated in Fig. 3(c). In such a rotation, ϕ is fixed at 0, while θ periodically changes, resulting in dynamical superpositions of $|T_+\rangle$ and $|T_-\rangle$ states.

For arbitrary qubit operations, it is necessary to rotate the qubit from one point to another on the Bloch sphere. This requires two-axis control, specifically controlling both θ and ϕ. To achieve this, an additional static magnetic field along the z-axis can be applied. When the instantaneous state is at $\theta = \pi/2$ ($|\Psi\rangle = (1/\sqrt{2})(|T_+\rangle + e^{i\phi}|T_-\rangle)$) pointing to either the A or B site, the static magnetic field B_z lifts the energy degeneracy between T_- and T_+ states. This results in a change in the oscillation frequency of the coherent superposition of

the STTE state. The energy difference between $|T_-\rangle$ and $|T_+\rangle$ states is $\Delta_E = g\mu_B B_z$. The STTE spin state then precesses around the z-axis by an angle $\phi = \Omega T^*$,[5,6] where the precession angular frequency ω is proportional to the energy splitting as $\Omega = \Delta_E/\hbar$. The coherence time T^* of $|T_+\rangle$ and $|T_-\rangle$ is 0.45 ns. Therefore, by combining the effects of the CPL and the static magnetic field, the STTE qubit can be coherently controlled along both the x and z axes. The range of B_z can be estimated as follows. The lower limit of B_z is determined by the requirement to implement a non-negligible phase gate within the qubit's coherence time T^*, which is

$$B_z \geq \frac{\phi\hbar}{g\mu_B T^*}. \tag{7}$$

To achieve a $\phi = \pi/2$ phase gate, we can estimate the lower limit of B_z to be about 0.02 T, which is a modest magnetic field in the laboratory. For the upper limit of B_z, it must ensure that the self-trapped structure of the exciton is not destroyed, namely, $\Delta_E \leq E_{\text{binding}} = 0.52t_0$. Then the upper limit of B_z is about 4 T.

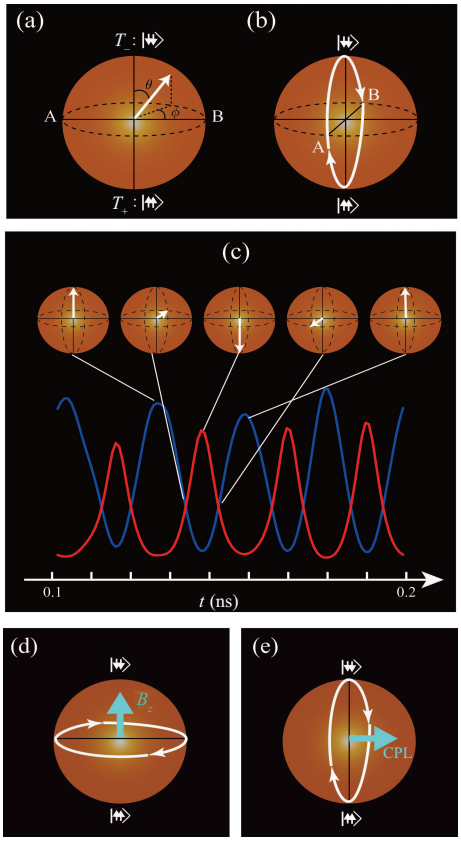


Fig. 3. (a) The Bloch sphere with the subspace constructed using the $|T_+\rangle$ and $|T_-\rangle$ states, where the A and B states are $(1/\sqrt{2})(|T_+\rangle - |T_-\rangle)$ and $(1/\sqrt{2})(|T_+\rangle + |T_-\rangle)$, respectively; (b) the rotations around the x-axis of the Bloch sphere which corresponds to the Rabi oscillations between the $|T_+\rangle$ and $|T_-\rangle$; (c) the instantaneous magnetization of the qubit state during Rabi oscillation; panels (d) and (e) are schematic view of the two-axis control by applying the static magnetic field and the CPL.

The spin state evolution induced by a CPL is a dynamical quantum phenomenon. To further clarify the detailed response of the lattice and spins to CPL, we demonstrate $\tilde{y}_i(t)$ and $S_{i,z}(t)$ in Fig. 4. In Fig. 4(a1), it is evident that the lattice-distortion envelope of the STTE remains intact for about 0.6 ns after the CPL is applied. The STTE's spins are tightly confined within the lattice-distortion envelope, effectively forming a CPL-manipulated QD system. The CPL-induced Rabi oscillation between the T_- and T_+ states can be observed by monitoring the evolution of $S_{i,z}(t)$. The $S_{i,z}(t)$ values alternately reach the positive and negative extremes, indicating that the STTE's spin is precessing around the x-axis. At around 0.6 ns, the decoherence between $|T_-\rangle$ and $|T_+\rangle$ takes place, which is accompanied by the detrapping of the STTE. The lattice-distortion envelope collapses and the spin density spreads over the whole chain. It can thus be inferred that stronger EL couplings enhance the coherence between $|T_-\rangle$ and $|T_+\rangle$. A more robust lattice-distortion envelope provides better resistance to external fields, thereby maintaining higher coherence. Figures 4(b1) and 4(b2) respectively show the evolution of $\tilde{y}_i$ and $S_{i,z}$ when the angular momentum of CPL is parallel to the initial spin orientation of STTE, where no Rabi oscillations take place. One can find that the lattice-distortion envelope remains unchanged and the spin does not oscillate, that is, the STTE does not respond to the CPL. The lattice-distortion envelope remains unchanged, and the spin does not oscillate, indicating that the STTE does not respond to the CPL. This behavior further highlights the helicity dependence of the STTE's response to the CPL.

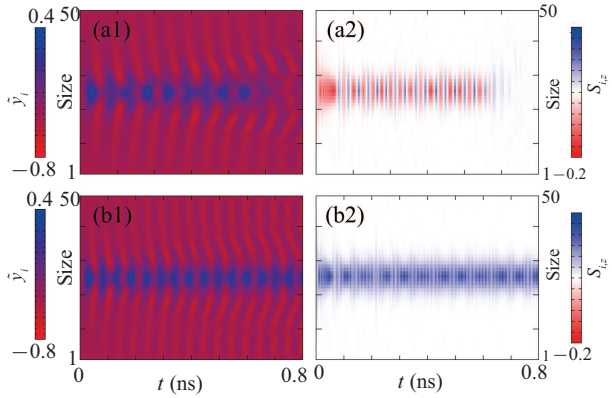


Fig. 4. Evolutions of $\tilde{y}_i$ and $S_{i,z}$, which respectively corresponds to the dynamics in Figs. 2(a) and 2(b).

4. Conclusion

In conclusion, we propose a theoretical framework for preparing and manipulating an STTE-based triplet-triplet qubit in organic materials. Due to the weak spin–orbit couplings in these materials, the spin state can be preserved for extended periods. Such an STTE qubit can be prepared in a prototype device, such as FM/polymer/FM sandwich structure. By applying a CPL, the spin state of the STTE can be coherently manipulated. The manipulation exhibits significant helicity dependence: when the angular momentum of CPL is

antiparallel to the initial state of the STTE, the Rabi oscillation between $|T_-\rangle$ and $|T_+\rangle$ is observed; when the angular momentum of CPL is parallel to the initial state, the STTE does not respond to the CPL. The CPL-driven Rabi oscillations between $|T_-\rangle$ and $|T_+\rangle$ correspond to the state rotation around the x-axis on the Bloch sphere. By additionally applying a static magnetic field B_z, state rotation around the z-axis can also be realized, enabling two-axis coherent control of the STTE qubit. Our work provides a theoretical foundation for exploring organic-based quantum computing devices. This approach leverages the unique properties of organic materials to offer promising avenues for developing robust and high-fidelity quantum information systems.

Data availability statement

The data that support the findings of this study are openly available in Science Data Bank at https://doi.org/10.57760/sciencedb.space.02183.

Acknowledgments

Project supported by the National Key Research and Development Program of China (Grant No. 2022YFF0503603), the Strategic Priority Research Program of the Chinese Academy of Sciences (Grant No. XDB1200200), and the Study Encouragement to Youth Innovation Promotion Association Outstanding Member of the Chinese Academy of Sciences (Grant No. Y2022057).

References

[1] Divincenzo D P 2000 *Fortschr. Phys.* **48** 771
[2] Veldhorst M, Yang C H, Hwang J C C, *et al.* 2015 *Nature* **526** 410
[3] Petta J R, Johnson A C, Taylor J M, *et al.* 2005 *Sciene* **309** 5744
[4] Kormanyos1 A, Zolyomi V, Drummond N D and Burkard G 2014 *Phys. Rev. X* **4** 011034
[5] Qu F Y, Braganca H, Vasconcelos R, *et al.* 2019 *2D Mater.* **6** 045014
[6] Wang G, Marie X, Liu B L, *et al.* 2016 *Phys. Rev. Lett* **117** 187401
[7] Nowack K C, Shafiei M, Lafores M, *et al.* 2011 *Science* **333** 6047
[8] Tusun M, Rong X and Du J 2019 *Chin. Phys. B* **28** 024204
[9] Bermeister A, Keith D and Culcer D 2014 *App. Phys. Lett.* **105** 192102
[10] Pei T, Palyi A, Mergenthaler M, *et al.* 2017 *Phys. Rev. Lett.* **118** 177701
[11] Mccamey D R, Seipel H A, Paik S Y, *et al.* 2008 *Nat. Mater.* **7** 723
[12] Palmer J R, Williams M L, Young R M, *et al.* 2024 *J. Am. Chem. Soc.* **146** 1089
[13] Shuai Z, Beljonne D, Silbey R J and Brédas J L 1999 *Phys. Rev. Lett.* **84** 131
[14] Zrenner A, Beham E, Stufler S, *et al.* 2002 *Nature* **418** 612
[15] Stievater T H, Li X, Steel D G, *et al.* 2002 *Phys. Rev. Lett.* **87** 133603
[16] Patton B, Woggon U and Langbein W 2005 *Phys. Rev. Lett.* **95** 266401
[17] Zhang L, Hao Y, Qin W, *et al.* 2020 *New J. Phys.* **22** 103034
[18] Su W P, Schriffer J R and Heeger A J 1979 *Phys. Rev. Lett.* **42** 1698
[19] Heeger A J, Kivelson S and Schrieffer J R 1988 *Rev. Mod. Phys.* **60** 781
[20] Zhang L and Hao Y 2021 *App. Phys. Lett.* **118** 093301
[21] Zhang L, Xie S and Kang D 2017 *Phys. Rev. E* **96** 022414
[22] Zhang L and Yamamoto S 2014 *J. Phys. Soc. Jpn.* **83** 064708
[23] Lu Q X, Ma X L, Gao T, Xie S and Qu F 2019 *Phys. Chem. Chem. Phys.* **21** 12924